Geophysical Journal International

Geophys. J. Int. (2015) **200,** 1555–1565 doi: 10.1093/gji/ggu490
GJI Marine geosciences and applied geophysics

Induced polarization of disseminated electronically conductive minerals: a semi-empirical model

Grigory Gurin,[1] Konstantin Titov,[1] Yuri Ilyin[1] and Andrey Tarasov[1,2]

[1] *Institute of Earth Sciences, St. Petersburg State University,* 7/9 *Universitetskaya naberezhnaya,* 199034 *St. Petersburg, Russia. E-mail: k.titov@spbu.ru*
[2] *"VIRG-Rudgeofizika" JSC,* 1, *Petrovskaya Kosa,* 197110 *St. Petersburg, Russia*

Accepted 2014 December 22. Received 2014 December 22; in original form 2014 June 6

SUMMARY

We studied artificial ore models that contained galena, pyrite, magnetite, graphite and cryptomelane with the time domain induced polarization technique. The models were mixtures of sand and metallic-type, electronically conductive mineral particles. We varied the volumetric content of the particles, their mineral composition and average grain size, as well as the pore water salinity. Based on the Debye decomposition approach, we obtained relaxation time distributions, which contained peaks. From these distributions, we obtained the total chargeability and the peak relaxation time. We correlated these parameters with the particle mineral composition, grain size, particle content and the pore solution resistivity. We also compared the experimental data with the Wong model prediction, which was unable to explain the entire data set. The above-mentioned correlations, in conjunction with some previously published data, allowed us to formulate a new, semi-empirical model that links (1) the total chargeability with the volumetric content of the particles and the total chargeability of the host matrix and (2) the time constant with the particle mineralogy, the particle radius and the pore solution resistivity.

Key words: Electrical properties; Electromagnetic theory.

1 INTRODUCTION

In the last decades, there has been an increased interest in the use of the induced polarization (IP) method in hydrogeology and contaminant hydrology (e.g. Kemna *et al.* 2012, and references therein). This interest stimulated development of field techniques and data inversion methodology, as well as of the spectral IP (SIP) approach, which studies IP parameters over a wide frequency range.

Recent experimental results were obtained mainly on soils and sediments, in order to assess their hydraulic conductivity, specific surface and grain size based on the IP parameters (e.g. Binley *et al.* 2005; Leroy *et al.* 2008; Weller *et al.* 2010). Very few data sets concerning disseminated minerals that represent electronic conductors or semiconductors (which we will call in this paper 'metallic particles') were obtained in the frameworks of environmental applications (Slater *et al.* 2005, 2006; Ntarlagiannis *et al.* 2010; Placencia-Gómez *et al.* 2013; Hubbard *et al.* 2014), investigations of archaeological objects (Florsch *et al.* 2011) and mining geology (Gurin *et al.* 2013, 2014).

However, starting from Schlumberger's research (Schlumberger 1920), IP has been traditionally used in mining geology for prospecting of disseminated ore (e.g. Scott & West 1969; Pelton *et al.* 1978; Nelson & Van Voorhis 1983; Vanhala & Peltoniemi 1992; Sigel *et al.* 1997). For instance, gold is frequently accompanied by disseminated sulphide minerals like pyrite and arsenopyrite, and IP anomalies are traditionally considered as indications of gold deposits (e.g. Andreev 1992; Hofstra & Cline 2000).

An idea to differentiate the mineral composition of metallic particles and the ore texture on the basis of SIP was proposed in several papers (Pelton *et al.* 1978; Vanhala & Peltoniemi 1992; Sigel *et al.* 1997). They based the differentiation approach on the experimentally obtained values of the IP magnitude and relaxation time. However, to date, there is no universal method for this differentiation. In this context, it is critically important to revise the previously obtained experimental data, to specify parameters determining the IP spectra, and to establish links between the spectral IP parameters and the rocks textural and physical–chemical properties.

Early laboratory experiments (e.g. Grissemann 1971; Mahan *et al.* 1986) were carried out in the context of mining geology, and provided spectral data sets obtained on synthetic models that contained grains of chalcopyrite and pyrite. Most of the models contained calibrated grains of the various sizes, and were saturated with solutions of the various salinity and chemical composition.

Recent experiments were carried out mainly in the framework of environmental applications. Placencia-Gómez *et al.* (2013) worked with pyrite and pyrrhotite. Their aim was to study the impact of mineral transformation on IP responses. Because they used a broad grain size distribution, their results are difficult to interpret in the ore texture context. Gurin *et al.* (2013) worked with composite particles of different sizes (particles contained pyrrhotite, pyrite,

magnetite and chalcopyrite), which makes it difficult to correlate the particle mineralogy to changes in the IP spectra. Slater *et al.* (2005) studied spectral IP responses of sand–iron particles mixtures with the varying particle content, and at different pore solution salinity levels, chemical compositions, and pH. However, the particle size was kept constant. Slater *et al.* (2006) obtained IP spectra on sand–magnetite mixtures at a single level of pore solution salinity, for one value of the particle radius size, and with the various values of the particle content. Hubbard *et al.* (2014) studied IP of magnetite, but their research was restricted to the influence on IP of the water chemical composition and pH.

In the context of the mineral differentiation, the above data are not systematic mainly because of the variability of particle mineral composition. However, these data enable us to identify major parameters influencing IP. These parameters will be discussed below.

The most popular models describing IP are the Cole–Cole model (Cole & Cole 1941) and the Pelton resistivity model (Pelton *et al.* 1978). Although these models fit numerous experimental data sets reasonably well, they are phenomenological; therefore, they do not provide direct links to textural, mineralogical and chemical parameters of disseminated ores.

Physical–chemical models were also proposed (Bulashevich 1956; Wait 1958; Marshall & Madden 1959; Alexeev *et al.* 1973; Wong 1979; Kormiltsev 1980). The most elaborate model, by Wong (1979), defines the relationship between IP parameters and physical–chemical properties of disseminated ores. However, that model contains eight independent parameters (some of which are hard to assess) and, therefore, it is difficult to compare the model predictions with the experimental data.

For the disseminated metallic particles three types of polarization can be considered. First, an external electrical field involves ion electro-migration and diffusion fluxes, which produces an excess or deficit of inactive ions (which are unable to cross the metal–electrolyte interface), so a concentration gradient appears. Then, a minor concentration of active ions existing in electrolyte enters in a redox reaction allowing the charge transfer across the metal–electrolyte interface. Additionally, the host medium also produces some polarization effect. We assume the host medium polarization is additive to the metallic particles polarization.

In this paper, we discuss the newly obtained IP data with very different minerals (galena, pyrite, graphite, magnetite and cryptomelane). We further investigate how the type of metallic mineral and its volumetric content in ion-conductive host media influence IP. We also discuss those experiments carried out while varying the pore water salinity level. We compare new data with the previously obtained results and with predictions of the Wong model, and we propose a simple semi-empirical model to describe the entire corpus of the experimental data.

2 IP PARAMETERS

IP is characterized by the magnitude and the relaxation time (or relaxation time distribution). It can be measured in frequency domain (FD) or in time domain (TD). In FD, the complex resistivity, conductivity or dielectric constant, measured over at least three decades of the frequency, are defined as IP spectra (e.g. Kemna *et al.* 2012). The IP intensity, polarization to conduction ratio, can be described by the electrical resistivity or conductivity dispersion, which produces the total chargeability defined as

$$M = \frac{\rho_0 - \rho_\infty}{\rho_0} = \frac{\sigma_\infty - \sigma_0}{\sigma_\infty}, \tag{1}$$

where $\rho_0 = \frac{1}{\sigma_0}$ and $\rho_\infty = \frac{1}{\sigma_\infty}$ are the low and high frequency limits of the resistivity, and σ_0, σ_∞ are the respective limits of the conductivity.

The magnitude of polarization is defined as the normalized total chargeability (e.g. Lesmes & Frye 2001; Slater *et al.* 2006),

$$M_n = M\sigma_0. \tag{2}$$

The relaxation time, τ, can be defied on the basis of a peak frequency, f_{peak}, in the imaginary component of the complex conductivity, which contains at least one peak:

$$\tau = \frac{1}{2\pi f_{\text{peak}}}. \tag{3}$$

When the peak is broad (like plateau), or when multiple peaks are observed, it becomes necessary to consider a relaxation time distribution. The peaks broadness depends, for instance, on the distribution of characteristic sizes of the polarisable elements in rocks and soils, such as colloidal particles, pores or metallic particles (e.g. Kemna 2000).

The relaxation time distribution can be obtained on the basis of the Debye decomposition (DD) approach (e.g. Morgan & Lesmes 1994; Nordsiek & Weller 2008). With this approach, one assumes that each textural element of rock or soil is polarized according to the Debye model, with its own intensity and characteristic time of polarization. As a result, in terms of electrical conductivity, this produces a superposition of polarization of the different textural elements:

$$\sigma(\omega) = \sigma_\infty \left(1 - \sum_j \frac{M_j}{1 + \mathrm{i}\omega\tau_j}\right), \tag{4}$$

where $i = \sqrt{-1}$, $\omega = 2\,\pi f$, $M_j = Z_j \Delta \ln \tau_j$ is the partial chargeability at a given relaxation time, τ_j, $\Delta \ln \tau_j$ is the sampling interval along the τ-axis in the logarithmic scale and $\sum_j M_j = M$ is, again, the total chargeability (see eq. 1). Assuming that the relaxation times are equally distributed in the logarithmic space, one recovers a relaxation time distribution, Z, which characterizes IP intensity versus relaxation time.

Because the asymptotic values in eq. (1) are difficult to assess, the total chargeability can be obtained based on the DD approach. It was determined as a sum of M_i (Nordsiek & Weller 2008) or as an integral of $Z(\tau)$ with respect to the natural logarithm of the relaxation time values (Tarasov & Titov 2007).

In TD, the IP is also characterized by the total chargeability and the normalized total chargeability. The local measure of IP is the polarizability, which is defined as the residual voltage, $U(t)$, produced by a current pulse, measured at a certain moment after the current is switched off, and normalized by the voltage value, U_p, observed during the current pulse. The time-averaged polarizability is defined as chargeability, which is a partial measure of the IP effect,

$$m = \frac{1}{U_p(t_{\max} - t_{\min})} \int_{t_{\min}}^{t_{\max}} U(t)\,\mathrm{d}t. \tag{5}$$

The values defined by eqs (1) and (5) are not the same. It is easy to show that the chargeability defined by eq. (5) depends on the τ value, while the total chargeability is not τ-dependent. Further in this paper, we use the total chargeability.

The relaxation time distribution can also be obtained from TD data based on the DD approach (Tarasov & Titov 2007), as well as the total chargeability. For metallic particles, this approach was tested in Nordsiek & Weller (2008) and in Gurin *et al.* (2013). In this

paper, we also apply it to the new data obtained on sand–metallic particle (SMP) mixtures, which model disseminated ores.

3 WHAT PARAMETERS CONTROL IP PRODUCED BY THE DISSEMINATED METALLIC PARTICLES?

In this section, we specify major factors determining the IP magnitude and relaxation time based on a literature review.

Slater *et al.* (2005) studied SMP mixtures with iron particles while varying the pore solution salinity, chemical composition and pH. They argue that the IP magnitude is determined by the specific surface of the particles, which was varied by changing the particle content. They found that the magnitude was almost independent of the pH value. For SMP with magnetite, Slater *et al.* (2006) also found an increase of the IP magnitude with increase of the specific surface area of the particles, produced by increasing their volumetric content. Mansoor & Slater (2007) found a linear relationship between the volumetric concentration of iron in clay and peat and the normalized chargeability obtained from the data fitting to the Pelton resistivity model. Nordsiek & Weller (2008) found a correlation between the mass concentration of slag grains and total chargeability. Based on measurements on the SMP mixtures with particles containing pyrrhotite, pyrite, magnetite and chalcopyrite (10 per cent), Gurin *et al.* (2013) suggested that the total chargeability was a universal measure of the particle volumetric content.

In a study of SMP mixtures, Slater *et al.* (2005, 2006) found different relaxation time values corresponding to iron and magnetite. For solutions of different chemical composition, they also obtained inverse relationships between the relaxation time and the activity of pore solution, which can be characterized by the electrical conductivity, σ_w:

$$\tau \sim \sigma_w^{-1}. \tag{6}$$

This relationship is completely different from the one for the insulating particles when the relaxation time is almost independent of the pore water conductivity (e.g. Schwartz 1962; Leroy *et al.* 2008).

For insulating particles, the quadratic relationship between the relaxation time and the grain diameter was established be several researchers (e.g. Schwartz 1962; Leroy *et al.* 2008). For metallic particles mixed with sand and fresh water, Gurin *et al.* (2013), based on both the previously published and the new data, found the relationship between the relaxation time and the grain radius, r, to also be quadratic:

$$\tau \sim r^2. \tag{7}$$

However, the proportionality coefficient for the insulating and metallic particles was found to be very different. This is, again, not consistent with the Schwartz (1962) theory, where that coefficient is proportional to the inverse of the ion diffusion coefficient.

For iron particles, a relationship between the relaxation time and pH was found unclear in Slater *et al.* (2005). They found a jump in the 'τ–pH' relationship and explained it by the pH-dependent surface charge of the iron surface. In a recent paper, Hubbard *et al.* (2014) found a relationship between the relaxation time of magnetite and pH of the pore solution. For redox-active ion Fe^{2+} in the pore solution, the relaxation time increased with the increase of the pore solution pH from 4 to 7. In contrast, for redox-inactive ions such as Ca^{2+} and Ni^{2+}, they found a constant relaxation time across the pH range from 4 to 10.

A relationship between the relaxation time and the shape of metallic particles was theoretically modelled in Wong & Strangway (1981). They showed that elongated oriented particles produced an anisotropic IP effect.

Recently published data suggest that the total chargeability of metallic-free sediments may achieve significant values at high specific surface area. For example, Weller *et al.* (2010) reported data obtained on a sandstone sample with the total chargeability of 0.27. Such total chargeability values are typical of metallic particles, and must be accounted for. Let us assess how the total chargeability of the host matrix influences the response of the mixture.

Let us consider a medium with low volumetric content of the particles allowing application of the Wagner mixture equation (e.g. Hanai 1968):

$$\frac{\sigma^* - \sigma_m^*}{\sigma^* + 2\sigma_m^*} = \frac{\sigma_p^* - \sigma_m^*}{\sigma_p^* + 2\sigma_m^*}\xi, \tag{8}$$

where ξ is the volumetric particle content, σ^*, σ_m^* and σ_p^* are the complex electrical conductivities of the mixture, matrix and particles, respectively.

For the case of DC, the particle conductivity is assumed to be zero, and for the infinite frequency it is assumed to be infinity (e.g. Wong 1979). Considering these limiting cases, one obtains after simple algebraic manipulations:

$$\sigma_0 = \frac{2\sigma_{0m}(1-\xi)}{2+\xi}, \tag{9}$$

$$\sigma_\infty = \frac{\sigma_{\infty m}(1+2\xi)}{1-\xi}, \tag{10}$$

$$M = 1 - (1 - M_m)\frac{2(1-\xi)^2}{(2+\xi)(1+2\xi)}, \tag{11}$$

where σ_{0m} and $\sigma_{\infty m}$ are the low and high frequency limits of the matrix conductivity, respectively, and M_m is the matrix total chargeability.

Therefore, the IP parameters mainly depend on the textural parameters (particle concentration, radius, shape and the host matrix texture), particle mineral composition, as well as on the pore solution chemistry, characterized by the salinity, chemical composition and pH (Fig. 1).

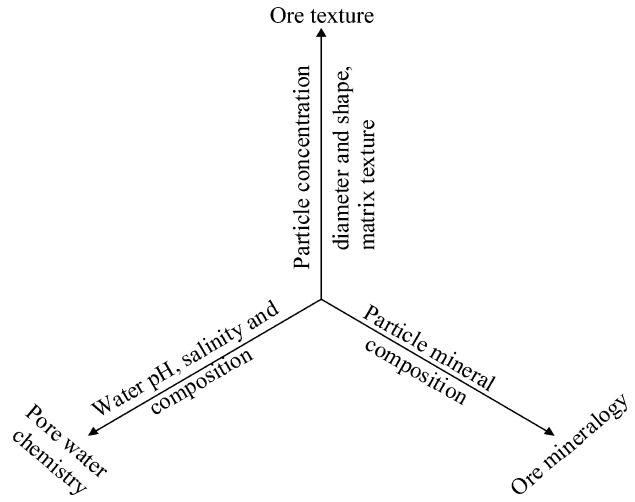

Figure 1. Parameters controlling the IP response of disseminated metallic particles.

In this paper, we systematically investigate roles of the above-mentioned factors by varying the mineral composition, particle volumetric content and grain size, as well as the pore water salinity determined by variations in NaCl concentration. However, we restrict our experiments to SMP mixtures. We also restrict our research to neutral (pH $\sim$ 7) solutions of NaCl. The particle shape and orientation are also excluded from consideration in our study.

4 METHODOLOGY OF EXPERIMENTS

We prepared 20 models of SMP mixtures that contained galena, pyrite, magnetite, cryptomelane and graphite. These minerals were of very different chemical composition and surface chemistry (two sulphides, two oxides and one native element), and were therefore considered as good samples for studying how the mineral composition influences the IP response.

Models that contained galena, magnetite and cryptomelane were investigated with the different levels of pore solution salinity in order to further study how the IP magnitude and relaxation time vary with the pore water salinity.

All SMP mixtures were made with calibrated particles of different average radii (obtained by sieving) to investigate the role of the particle average size. We also varied the particle volumetric content, and we investigated models containing mixture of particles: (1) with different radii and (2) with the same radius and different mineralogical composition to study IP responses in cases of complex texture and mineralogy. The sample porosity values after packing were 0.4 ± 0.05 (determined by weighting), and their bulk density ranged from 1.97 g cm^{-3} (for the blank sample containing water-saturated sand only) to 2.57 g cm^{-3} for the sample containing 12 per cent of galena. Obviously, the model bulk density increased with the increase of the metallic particle content and of the mineral density.

All models investigated in this paper, as well as the published data used to compare with the new data, are summarized in Tables 1 and 2.

Table 1. Mono-mineral models: summary of the experimental and published data.

Minerals and their volumetric content, ξ (per cent)	r (mm)	σ_w (mSm^{-1})	M (dimensionless)	τ (s)	Model electrical conductivity (mSm^{-1})
Mono-mineral models					
Galena, 10	0.55	105	0.39	0.7×10^{-3}	33.1
		51.9	0.34	2.7×10^{-3}	13.3
		20	0.39	9.9×10^{-3}	4.76
		11.0	0.39	2.0×10^{-2}	2.65
		5.00	0.40	4.6×10^{-2}	1.28
		2.50	0.40	8.0×10^{-2}	0.77
Magnetite, 12	0.55	200	0.54	1.0×10^{-3}	48.2
		100	0.46	$2.2.0 \times 10^{-3}$	25.1
		50	0.47	$4.5.0 \times 10^{-3}$	13.3
		10	0.51	1.0×10^{-2}	3.05
Magnetite, 10	0.55	20	0.39	1.2×10^{-2}	4.42
Pyrite, 10	0.55	20	0.32	2.5×10^{-2}	4.51
Graphite, 10	0.55	20	0.34	8.0×10^{-2}	4.25
Cryptomelane, 10	0.2	100	0.34	2.0×10^{-2}	24.8
		20.6	0.39	7.0×10^{-2}	5.25
		9.90	0.42	1.6×10^{-1}	2.74
		3.96	0.46	4.1×10^{-1}	1.25
		2.53	0.45	4.8×10^{-1}	0.95
Published data					
Chalcopyrite, 6.5 (Mahan *et al.* 1986)	0.138	66.6	0.28	4.0×10^{-4}	20.4
		19.4	0.23	8.0×10^{-3}	10.3
		9.4	0.25	4.0×10^{-3}	3.20
Chalcopyrite, 9 (Mahan *et al.* 1986)	0.049	59.5	0.43	8.0×10^{-5}	14.6
		8.8	0.38	2.0×10^{-4}	59.7
		2.1	0.34	1.2×10^{-3}	14.7
Pyrite, 6.3 (Mahan *et al.* 1986)	0.049	6.6	0.28	1.1×10^{-3}	6.00
Zero valent iron, 5 (Slater *et al.* 2005)	0.2	17	0.30	1.1×10^{0}	4.00
		83	0.21	3.8×10^{-1}	12.3
		164	0.24	2.2×10^{-1}	27.4
		750	0.25	4.6×10^{-1}	126
		6450	0.19	7.0×10^{-3}	991
		13400	0.22	2.4×10^{-3}	1837.30
Magnetite, 15 (Slater *et al.* (2006)	0.2	91	0.22	1.5×10^{-4}	2.50

Table 2. Composite models: summary of the experimental data.

Volumetric content, ξ (per cent)		r (mm)		σ_w (mSm^{-1})	M (dimensionless)	τ (s)		Model electrical conductivity (mSm^{-1})
Galena–Galena								
ξ_1	ξ_2	Gal	Gal			τ_1	τ_2	
2	–	0.045	0.55	20	0.092	1.3×10^{-4}	–	5.10
2	2	0.045	0.55	20	0.16	–	8.9×10^{-3}	5.51
2	4	0.045	0.55	20	0.22	0.9×10^{-4}	7.2×10^{-3}	5.39
2	6	0.045	0.55	20	0.25	2×10^{-4}	10×10^{-3}	5.39
2	8	0.045	0.55	20	0.35	1.8×10^{-4}	9.7×10^{-3}	5.51
4	8	0.045	0.55	20	0.37	1.9×10^{-4}	7.9×10^{-3}	5.28
Galena–Cryptomelane								
ξ_3	ξ_4	Gal	Cryp			τ_3	τ_4	
2	–	0.125	0.55	20	0.08	8.3×10^{-4}	–	5.67
2	2	0.125	0.55	20	0.21	6.3×10^{-4}	0.36	5.63
4	2	0.125	0.55	20	0.28	6.6×10^{-4}	0.42	5.49
6	2	0.125	0.55	20	0.24	6.6×10^{-4}	0.38	5.39
6	4	0.125	0.55	20	0.29	6.6×10^{-4}	0.32	5.03
6	6	0.125	0.55	20	0.36	6.7×10^{-4}	0.35	5.60
8	6	0.125	0.55	20	0.39	7.4×10^{-4}	0.33	5.30

Note: ξ and τ are volumetric contents of the minerals and the relaxation times, respectively. Subscripts: 1 — for galena with particle radius 0.045 mm; 2 — for galena with particle radius 0.55 mm; 3 — for galena with particle radius 0.125 mm; 4 — for cryptomelane with particle radius 0.55 mm.

5 MATERIALS AND METHODS

We used mixtures of sieved sand (0.2–0.3 mm), with crushed and sieved natural galena, magnetite, pyrite and cryptomelane, as well as 'technical' (artificial) graphite. The grain average size ranged from 0.045 to 0.55 mm.

The mineral samples were taken from the different deposits. Thus, galena was taken from the Zyryanovskoe deposit (Altai), pyrite—from the Parandol deposit (Karelia), magnetite—from the Kovdor deposit (Kola Peninsula), and cryptomelane—from the Karazhalskaya group of deposits (Kazakhstan). The 'technical' porous graphite we used had been produced for electrode manufacturing. We selected it because this material was mineralogically pure.

The commercial sand from a quarry in the St Petersburg region, Russia, consisted (by volume) of 73 per cent quartz, 26 per cent feldspar and 1 per cent other minerals. The pore solution was NaCl with electrical conductivity ranging in different experiments from 2.50 to 200 mSm^{-1} at room temperature of 22 °C (the salinity varied between 1400 and 16.9 mg l^{-1}).

The sand and the crushed ore minerals were separately washed with distilled water to remove the dust particles. Then the materials were oven-dried, and the crushed ore minerals were mixed with the sand. The mixtures were placed into a measuring cell, which was filled with NaCl solution from bottom to top. At least 20 volumes of the pore space were flushed with the solution. The control of chemical equilibrium between the mixtures and the solution was obtained by measuring the effluent solution conductivity values (DIST-4, Hanna Instruments), which were found very close to those of the influent solution. Then IP measurements were carried out. In those experiments where the solution salinity changed, the samples were flushed again with more saline solution prior to recommencing IP measurements.

The measurement cell was a PVC tube 18 cm long, with the inner diameter of 24 mm (Fig. 2). It was equipped with two brass ring current electrodes and two Ag/AgCl potential electrodes. The potential electrodes were connected to the tube trough low-salinity salt bridges to prevent sample contamination by the electrode solution.

For the IP measurements, we used an AIE-2 commercial TD field instrument (http://www.environmental-expert.com/products/aie-2-instruments-245668) and a low current transmitter custom-made for laboratory experiments. This equipment, as well as the measurement procedure and calibration experiments, were described in detail in Gurin *et al.* (2013).

During the experiments, we obtained IP decays as arithmetic average values of three independent measurements. Then we approximated the experimental decays by a set of exponential decays with the various magnitude and relaxation times. This approximation allowed us to reduce the random noise, to obtain smoothed decays, and to interpolate the voltage values on the logarithmic timescale. Then, on the basis of the smoothed decays, we calculated RTDs according to the Debye decomposition approach. Details concerning application of the DD approach to TD data can be found in Tarasov & Titov (2007), and its application to SMP mixtures in Gurin *et al.* (2013).

6 RESULTS

6.1 Total chargeability and normalized total chargeability

Fig. 3 shows how the total chargeability varies with the particle volumetric content. According to the previous results (e.g. Pelton *et al.* 1978; Slater *et al.* 2005; Gurin *et al.* 2013), the total chargeability increases with the particle content increase. In Fig. 3, we also plotted predictions derived from eq. (11).

Most of the data points fall between the prediction of the Wong model (based on the assumption that the host rocks are non-polariziable) and the theoretical graph for the host medium with the total chargeability of 0.04, which is typical of sand filled with fresh water. Data obtained with pyrite (Pelton *et al.* 1978) represent an exception and correspond to larger chargeability values.

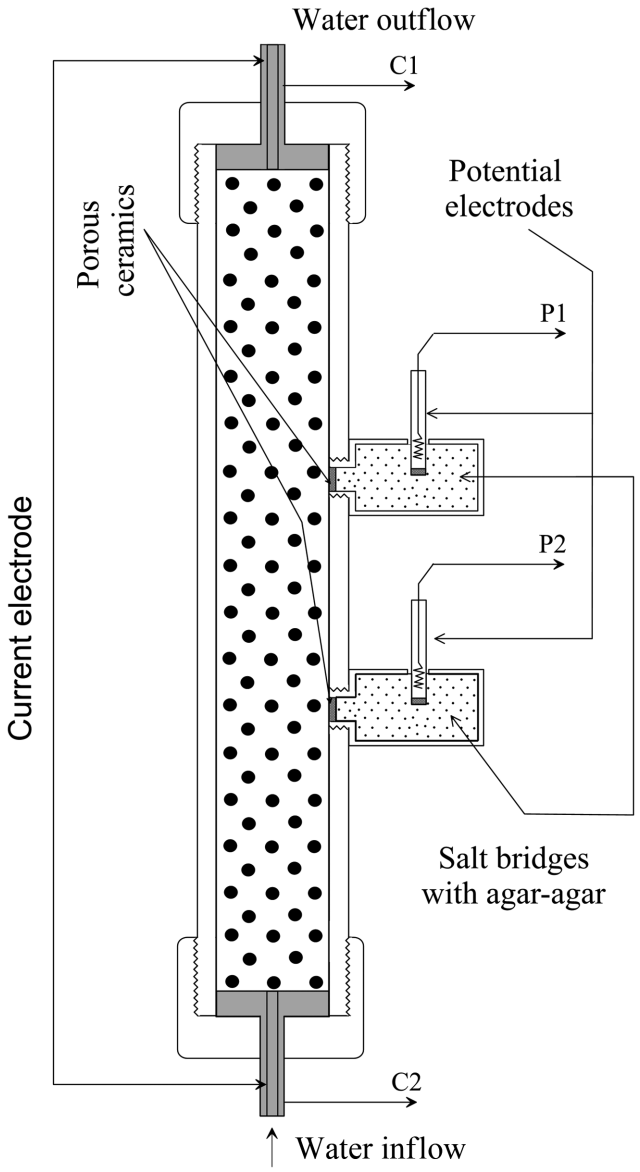

Figure 2. Schematic representation of the experimental system.

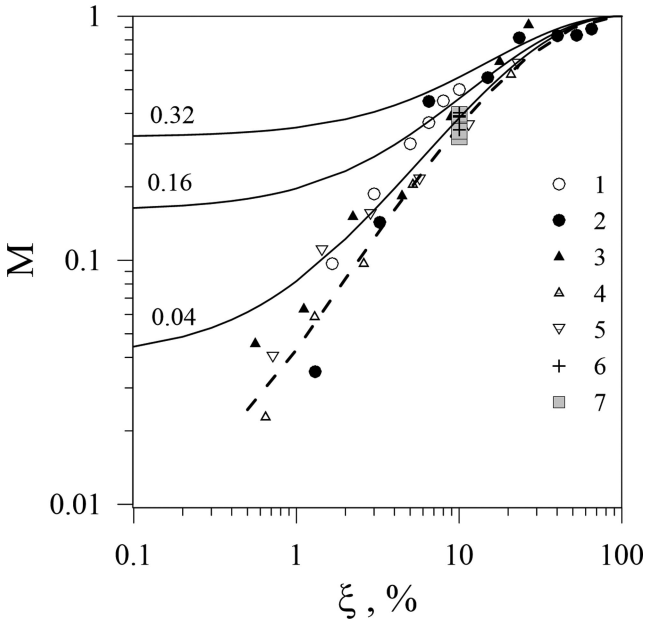

Figure 3. Total chargeability versus particle volumetric content for various particle radii, mineral composition and salinity of the pore solution. 1. Pyrite (0.2–0.3 mm) (Pelton *et al.* 1978); 2. Fe (0.2 mm; 850 mg l^{-1}) (Slater *et al.* 2005); 3. Mixture of pyrite, pyrrhotite, magnetite (0.55 mm, 135 mg l^{-1}) (Gurin *et al.* 2013); 4. Mixture of pyrite, pyrrhotite, magnetite (0.125 mm, 135 mg l^{-1}) (Gurin *et al.* 2013); 5. Mixture of pyrite, pyrrhotite and magnetite (0. 045 mm, 135 mg l^{-1}) (Gurin *et al.* 2013); 6. Galena with grain sizes 0.55 and 0.045 mm, 17 mg l^{-1} (this work); 7. Different mineral composition: galena, pyrite, magnetite, technical graphite and cryptomelane, constant volumetric content (10 per cent), particle radii (0.55 mm) and pore water salinity (135 mg l^{-1}). Solid lines show the total chargeability as a function of the host matrix total chargeability (M_m is shown by numbers), and the dashed line shows the Wong model prediction.

However, Pelton *et al.* (1978) used the experimental data of Grissemann (1971), which were obtained on artificial rocks composed of cement and pyrite particles, and we believe the total chargeability of the cement was higher than that of the sands.

An increase of the solution salinity produced increased values of the total normalized chargeability, which can be approximated by a linear fit (Fig. 4). Some scattering is produced by the different particle concentrations included in this data set. Our data agree well with those obtained with the SMP mixtures containing iron particles (Slater *et al.* 2005). For comparison, we show the total normalized chargeability of a sandstone sample, which slightly increases with the solution salinity (the power law exponent is 0.4), which is quantitatively in accordance with the previously published data (e.g. Weller *et al.* 2010; Revil *et al.* 2013).

6.2 Relaxation time

Relaxation time distributions obtained with the galena mixtures containing various grain radii (Fig. 5) have one maximum each. All distributions have very similar shapes, but they are mutually displaced along the τ-axis. The coarser is the grain, the higher is the relaxation time value. This is in agreement with the results obtained in previous experiments (e.g. Grissemann 1971; Mahan *et al.* 1986; Gurin *et al.* 2013).

Fig. 6(a) shows relaxation time distributions obtained in the experiments with galena particles of the same radius (0.55 mm) and particle concentration (10 per cent), but with the varying salinity of the pore water. As in the previous case, the graph shapes are very similar, and they are shifted along the τ-axis: the higher is the solution salinity, the lower is the relaxation time. This is also in agreement with the previous experiments (Slater *et al.* 2005). For comparison, in Fig. 6(b) we plotted the prediction of the Wong model as the imaginary conductivity spectra. Same as in the previous case, with the increased salinity, the maxima shift toward the lower values of the reciprocal of angular frequency. However, in contrast to the experimental distributions with increased salinity, the imaginary conductivity shows an increase of the magnitude and a decrease of the peak width. Moreover, the insert in Fig. 6(b) shows the strong difference in the '$\tau - \sigma_w$' relationship obtained experimentally and predicted by the Wong model.

Fig. 7 shows RTDs obtained with the different mineralogical compositions of the particles, with all other parameters kept unchanged. Regarding the peak position, the investigated minerals present the following series (in order of increased τ-values): galena–magnetite–pyrite–graphite–cryptomelane. The peak magnitudes are different, but the total chargeability values obtained in these experiments are

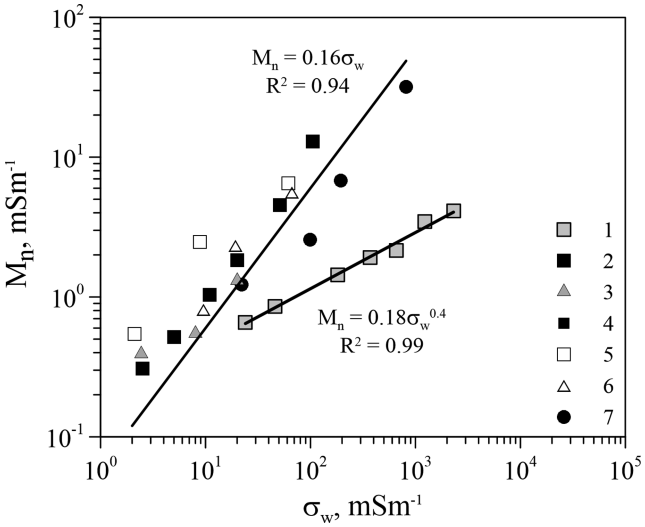

Figure 4. Normalized total chargeability versus water salinity (NaCl). 1. Sandstone sample Bu3 (Weller *et al.* 2011); 2. Galena — 0.55 mm, 10 per cent (this work); 3. Galena — 0.125 mm, 10 per cent (this work); 4. Cryptomelane — 0.2 mm, 10 per cent (this work); 5. Chalcopyrite — 0.45 mm, 9 per cent (Mahan *et al.* 1986); 6. Chalcopyrite — 0.053 mm, 6.5 per cent (Mahan *et al.* 1986); 7. Fe — 0.2 mm, 5 per cent (Slater *et al.* 2005). Two best fits are shown: for ion-conductive sample and for SMP mixtures.

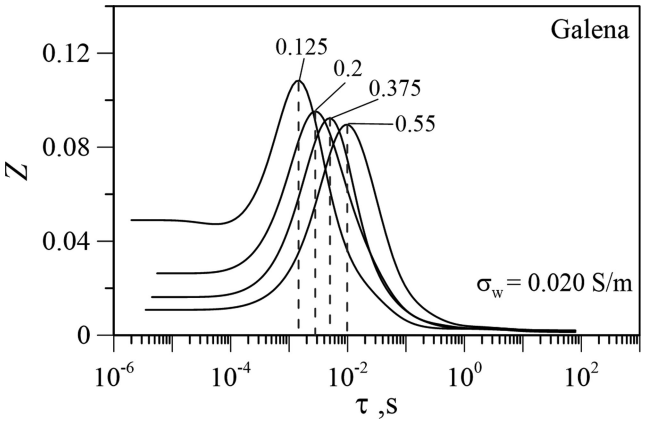

Figure 5. Relaxation time distribution for models containing 10 per cent of galena with different particle radii shown by numbers (in millimetres) and with the pore water salinity of 135 mg l^{-1} of NaCl ($\sigma_w = 0.020$ Sm^{-1}).

very close (except for magnetite, where the total chargeability was found to be about 25 per cent higher than the average value).

Fig. 8 shows relaxation time distributions obtained on composite models. In one experiment, galena of two different grain sizes was mixed with sand in different proportions. For these models, bimodal RTDs with peaks at 2×10^{-4} s and 10^{-2} s were obtained (Fig. 8a). The left peak's magnitude increases with the increase of the small particle concentration, and the right peak's magnitude—with the increase of the large particle concentration. The total chargeability is determined by the total concentration of galena.

In another experiment (Fig. 8b), two minerals (galena and cryptomelane) were mixed with sand in different proportions. The relaxation time distributions show, again, two distinct peaks at 7×10^{-4} s and 0.35 s. The left peak's magnitude increases with the increase of the galena concentration, and the right peak's magnitude—with the increase of the cryptomelane concentration. The peaks are of similar shape, and their magnitudes depend on the volumetric content of the corresponding particles. The total chargeability is, again, determined by the total concentration of metallic particles.

7 DISCUSSION

Within the limit of 10 per cent of the particle content (which is of principal interest for IP studies), the total chargeability of SMP mixtures linearly increases with the increase of the metallic particle content (Fig. 3), with a minor dependency on the solution salinity, particle mineralogy and size. This is in accordance with the previous experimental findings by Slater *et al.* (2005, 2006), Nordsiek & Weller (2008) and Gurin *et al.* (2013). The chargeability is well predicted by the Wong model. However, for larger chargeability values of the host matrix, the theoretical graphs are non-linear, and the graph slopes vary with the particle content and the host matrix total chargeability. Therefore, with increase of the matrix chargeability, the sensitivity of the total chargeability to the particle content decreases.

In contrast to the cases of ion-conducting sediments, the normalized total chargeability is proportional to the pore water salinity (Fig. 4) and, accordingly, the total chargeability is independent of the salinity. Considering these different relationships for the ion-conducting matrix and the metallic particles, the relative matrix effect should decrease with the increase of the water salinity.

As compared with the total chargeability, the 'chargeability–particle content' relationship presents a scattering (not shown). This fact is explained by the difference between the parameters. The total chargeability (as the integral parameter of IP spectra) is independent of the relaxation time value, while the chargeability depends on the relaxation time, which varied in our experiments subject to the particle size, mineralogy and pore solution salinity.

In accordance with the previous results (e.g. Mahan *et al.* 1986; Slater *et al.* 2005) the relaxation time is inversely related to the pore solution salinity and, therefore, to the electrical conductivity. This relationship is different from the case of ion-conductive sediments, where the relaxation time is almost independent of the solution salinity (e.g. Weller *et al.* 2011).

The relaxation time is controlled by the metallic grain radius. When the different data sets are fitted with power laws, the power values are found to be between 1.3 (this work, galena, 0.125–0.55 mm) and 2.3 (Grissemann 1971, chalcopyrite, 0.04–0.2 mm). A quadratic relationship fits the data fairly well (e.g. Gurin *et al.* 2013). Some scattering can be explained by differences in solution salinity and grain mineralogy. Therefore, a quadratic relationship is a reasonable approximation for the dependence of the relaxation time on the grain size. However, these experimental results partially disagree with the Wong (1979) model, which predicts two relationship domains: quadratic for large particle radii and linear for the small radii. Experimental data on the relationship between the relaxation time and the solution salinity are also in disagreement with the Wong model prediction (Fig. 6).

Data shown in Fig. 8 and Table 2 suggest that the relaxation time is independent of the chargeability. This is in disagreement with the results obtained in Pelton *et al.* (1978) on the basis of their resistivity model. We believe that this disagreement is produced by the different methodology of calculating the relaxation time. As was recently shown in Tarasov & Titov (2013), in contrast to the Cole–Cole model (Cole & Cole 1941), in the Pelton model τ depends on the chargeability and the exponent, c. This is especially pronounced at large chargeability values typical of metallic particles. However, for partial chargeability values, $Z(\tau)$, obtained with the Debye decomposition approach, both models give very similar results.

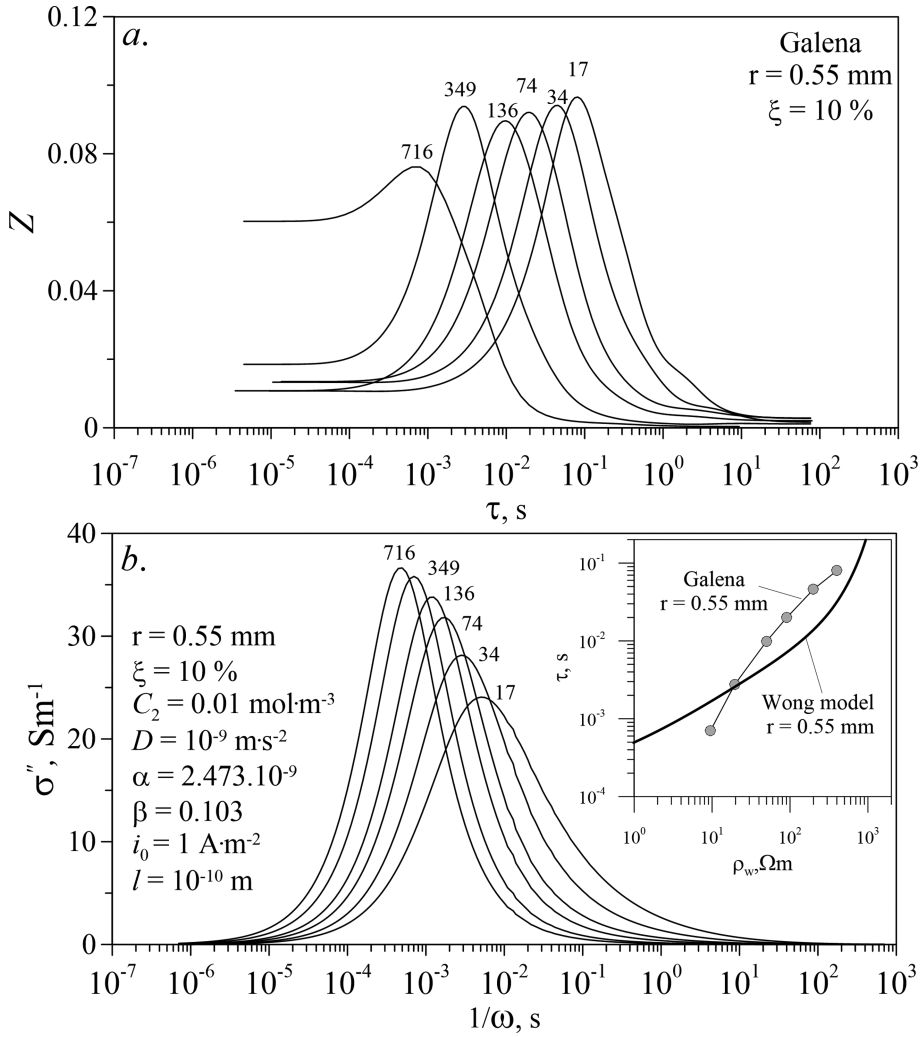

Figure 6. (a) RTD of the models with galena particles ($r = 0.55$ mm, $\xi = 10$ per cent), and (b) imaginary complex conductivity versus $1/\omega$, as predicted by the Wong model for the various salinity levels of the pore solution shown by numbers (in mg l^{-1}). The Wong model parameters are: C_2 — the concentration of specific ions participating in the redox reactions; D — the diffusion coefficient; i_0 — the equilibrium constant current density; l — the thickness of the Helmholtz layer; α and β are the electrochemical reaction current parameters. An insert in Fig. 6(b) shows relationships between the peak relaxation time and the pore solution salinity from the experimental data and as predicted by the Wong model.

The relaxation time was also found to be strongly related to the particle mineralogy (Figs 7 and 8). In Fig. 9, we highlight this relationship for each mineral by plotting the relaxation time normalized by the grain radius square as a function of the pore solution electrical resistivity. For all minerals, the parameters are proportional. We also plotted the prediction of the Wong model. The solid line corresponds to the common parameters of the model we used previously in this paper (shown in Fig. 6) except for the solution electrical resistivity, whose value we varied. However, most of the experimental data points fall upward of the model prediction. We varied the model parameters, and we found that the area of experimental points can be enclosed by the model graphs only assuming that the diffusion coefficient varies between 10^{-9} m^2 s^{-1} (solid line) and 10^{-12} m^2 s^{-1} (dashed line). The last value is three orders of magnitude smaller than that for the ions in the free solution, presumed in the model. Therefore, regarding the relaxation time, the data disagree with the model prediction.

Data shown in Fig. 9 suggest that the experimental results concerning the grain radius, the pore solution electrical resistivity, ρ_w and the mineral composition of the particles can be combined in a simple empirical equation describing the above-mentioned relationships of the relaxation time:

$$\tau = a\frac{r^2}{\sigma_w} = ar^2\rho_w, \tag{12}$$

where the coefficient, a (with dimension of Fm^{-3}) characterizes the volumetric specific capacitance of the rock dependent on the particle mineralogy and surface chemistry. In Fig. 9, for galena, magnetite and chalcopyrite, we calculated a common fit; however, the data allowed us to calculate the values of the a-coefficient for the individual minerals based on eq. (12) (Table 3).

Table 3 and Fig. 9 show that the specific capacitance varies with mineralogy and is, at the first approximation, independent on the pore water salinity, the grain radius and the particle concentration. For magnetite and pyrite, we calculated the values of the coefficient based on the different data sets. For instance, for magnetite, data obtained in this work and published in Slater *et al.* (2006) give the a-values of the same order of magnitude. Similarly, the values of the coefficient calculated for pyrite based on this work and on the data

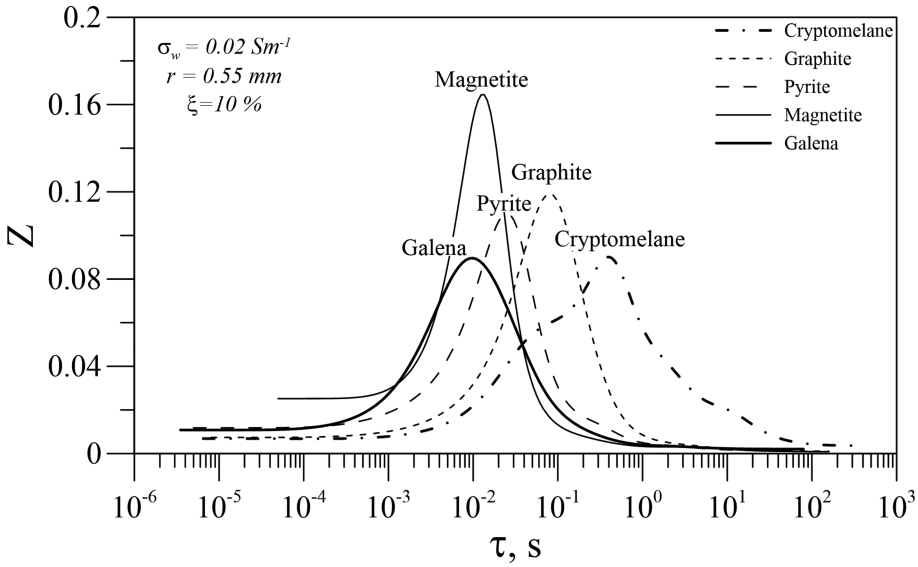

Figure 7. RTD obtained with the different mineralogical compositions of the particles, and the same volumetric particle content (10 per cent), the grain radius (0.55 mm) and the pore solution salinity (135 mg l^{-1}).

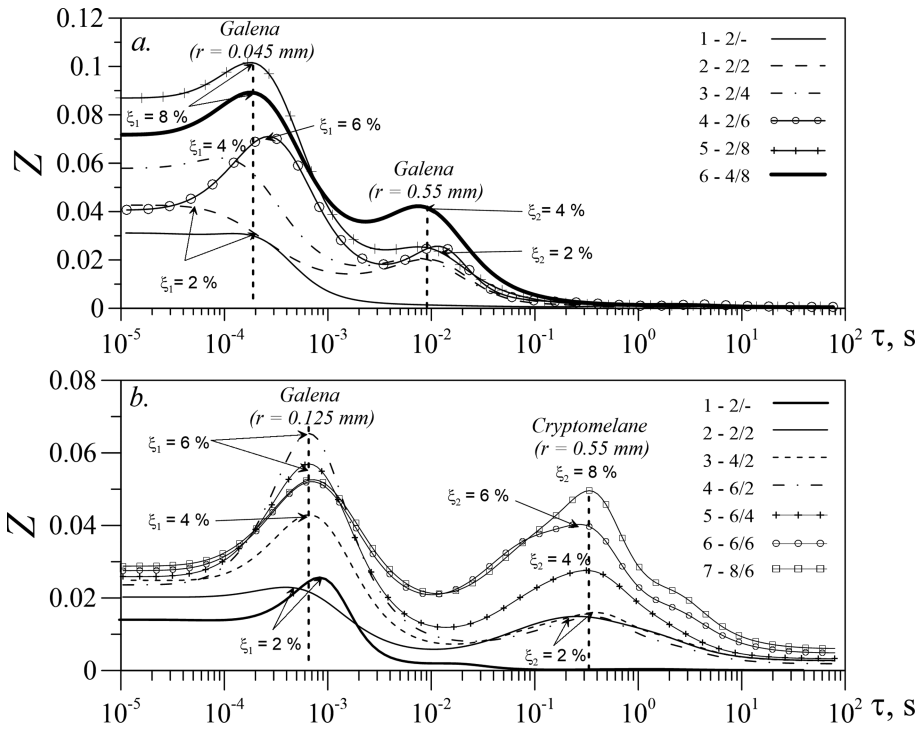

Figure 8. RTD obtained for composite models. (a) Particles of galena with different radii (0.045 and 0.55 mm). (b) Particles of galena (0.125 mm) and cryptomelane (0.55 mm). The pore solution salinity is 135 mg l^{-1}. The particle content is shown by fractions $\frac{\xi_1}{\xi_2}$, where subscripts 1 and 2 are related to the content of the smaller and the larger particles.

obtained by Mahan *et al.* (1986) are close. This data comparability confirms our approach based on eq. (12).

In order of increase of the coefficient value, the minerals present a series from galena and magnetite to zero valent iron (Table 3). Low-stability minerals (magnetite and sulphides) show relatively low values of the coefficient (7×10^2–3×10^3 Fm^{-3}), and stable minerals (graphite and cryptomelane) show higher values of the coefficient (6×10^3–3.2×10^4 Fm^{-3}). Zero valent iron (which is not stable) shows the highest value of the coefficient 4.6×10^5 Fm^{-3}, which is an exception. Another attempt to interpret this series is to relate the mineral position in the series to the electrochemical properties of its interface. From literature (Ilyin 1968; Ilyin *et al.* 1980; Suhotin 1981), we obtained the values of the mineral electrode potential (φ), and we correlated them to the *a*-coefficient values. Fig. 10 shows a reasonable data fit except for graphite. This exception is probably related to the internal porosity of the artificial graphite we used in experiments.

For a mono-modal distribution of particle sizes, and for a mono-mineral particle composition, the relaxation time distribution is also mono-modal and typically symmetric [except for one case detected for cryptomelane (Fig. 7)]. Therefore, the polarization can be described by the simple Cole–Cole model, and is

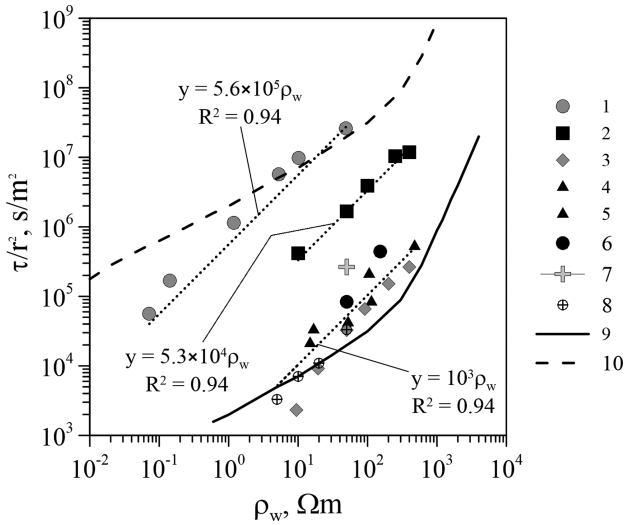

Figure 9. Relaxation time normalized to by the particle radius square versus pore solution electrical resistivity for different minerals. 1. Fe, $r = 0.2$ mm, 5 per cent (Slater *et al.* 2005); 2. Cryptomelane, $r = 0.55$ mm, 10 per cent (this work); 3. Galena, $r = 0.2$ mm, 10 per cent (this work); 4. Chalcopyrite, $r = 0.45$ mm, 6 per cent (Mahan *et al.* 1986); 5. Chalcopyrite, $r = 0.053$ mm, 9 per cent (Mahan *et al.* 1986) 6. Pyrite, 10 per cent (this work); 7. Graphite 10 per cent (this work); 8. Magnetite $r = 0.55$ mm, 12 per cent (this work). For galena, magnetite and chalcopyrite a common proportionality fit is defined. For other minerals, individual fits are presented. 9 and 10 are predictions of the Wong model for the different diffusion coefficient values (9. $D = 10^{-9}$ m^2 s^{-1}; 10. $D = 10^{-12}$ m^2 s^{-1}, $r = 0.2$ mm other parameters are shown in Fig. 6).

Table 3. Volumetric specific capacitance of the minerals.

Mineral	a (Fm^{-3})	R^2
Magnetite[a,b]	3×10^2	–
Magnetite	6.5×10^2	0.996
Galena	7.3×10^2	0.998
Chalcopyrite[c]	1.4×10^3	0.968
Pyrite[b,c]	2.8×10^3	–
Pyrite[b]	3.0×10^3	–
Graphite[b]	6.0×10^3	–
Cryptomelane	3.2×10^4	0.977
Fe[d]	4.6×10^5	0.971

Note: R^2 is the determination coefficient.
[a]Data from Slater *et al.* (2006).
[b]Calculated on the basis of τ characterized by one or two points.
[c]Data from Mahan *et al.* (1986).
[d]Data from Slater *et al.* (2005).

characterized by the chargeability, the relaxation time and the exponent, c. The chargeability can be computed from eq. (11). The time constant can be obtained from eq. (12). In our experiments, the Cole–Cole exponent values were found to be between 0.5 and 0.7 (data not shown). For the cryptomelane case, the exponent c was found to be close to 0.5; for graphite and galena—0.6; and for magnetite and pyrite—0.7 (see Fig. 7 showing different breadth of the peaks in the RTD). However, we found it difficult to relate the exponent to the physical–chemical parameters of the models because the broadness of the particle size distribution within each class was not assessed. This could become a subject of a separate study.

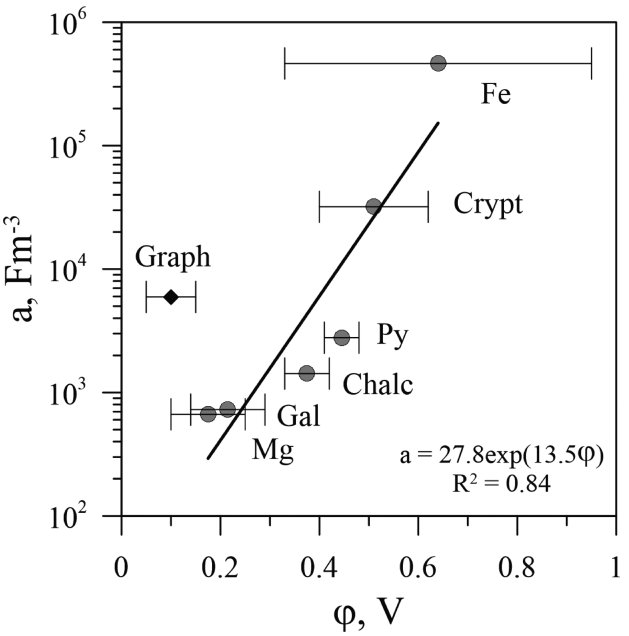

Figure 10. Relationship between the volumetric specific capacitance (a) of the minerals (this work) and the electrode potential relative to the calomel electrode (from published data).

8 CONCLUSIONS

In this paper, we studied the IP behaviour of the different minerals in NaCl solution that contained a small amount of specific ions that were able to reduce or oxidize in the electrical field and in the presence of metallic particles. These ions can appear in the solutions because, for example, of dissolution of the particles. In the above conditions, the chargeability and the time constant depend on the ore texture, mineralogy and the pore solution chemistry in the following way. The total chargeability is calculated according to the Wagner mixing law (eq. 11). The time constant can be obtained from eq. (12). The coefficient a in eq. (12) is a property of a mineral nearly independent of the particle concentration, radius and pore solution salinity. Eqs (11) and (12) present the new semi-empirical model, characterizing the IP total chargeability and relaxation time of disseminated metallic particles.

The presented data agree with the Wong model regarding the total chargeability behaviour. However, the data concerning the relaxation time are in disagreement with the model prediction.

From the practical point of view, serious limitations in the use of SIP in the mineral differentiation occur because the relaxation time depends on three parameters. Within a typical survey area, the pore water salinity (and electrical conductivity) values can be considered constant. However, even if this is true, the particle size can be assessed assuming unvaried mineral composition of ores. Such an assessment was recently obtained in Gurin *et al.* (2014). Assuming that gold was correlated with the pyrite content, they qualitatively assessed the pyrite grain size based on field TD IP data. Alternatively, minerals can be differentiated only assuming the same shape and size of the metallic particles.

ACKNOWLEDGEMENTS

We thank the Editor Mark Everett, Nicolas Florsch and an anonymous reviewer for their constructive comments. This work was supported by St Petersburg State University (Grants 3.0.114.2010

and 3.37.134.2014). Equipment of Core Facility RC 'Geomodel' of St Petersburg State University was used in this work.

REFERENCES

Alexeev, A.I., Merkushev, A.M. & Lavrov, I.S., 1973. Elektrohimicheskay polarizaciy provodyashih sfer v rastvore electrolitov, *Kolloidniy jurnal, Moscow,* **34,** 620–626 (in Russian).

Andreev, B.S., 1992. *Pirit zolotorudnyh mestorozhdeniy,* Nedra Press, 141 pp. (in Russian).

Binley, A., Slater, L.D., Fukes, M. & Cassiani, G., 2005. Relationship between spectral induced polarization and hydraulic properties of saturated and unsaturated sandstone, *Water Resour. Res.,* **41,** W12417, doi:10.1029/2005WR004202.

Bulashevich, Yu.P., 1956. Raschet polya vizvaniyh potencialov dlya rudnih tel sfericheskoy formi, *Izv. AN SSSR, Ser. Geophizika,* **5,** 504–512.

Cole, K.S. & Cole, R.H., 1941. Dispersion and absorption in dielectrics — I. Alternating current characteristics, *J. Chem. Phys.,* **9,** 341–351.

Florsch, N., Llubes, M., Téreygeol, F., Ghorbani, A. & Roblet, P., 2011. Quantification of slag heap volumes and masses through the use of induced polarization: application to the Castel-Minier site, *J. Archaeol. Sci.,* **38,** 438–451.

Grissemann, C., 1971. Examination of the frequency-dependent conductivity of ore-containing rock on artificial models, Sc. Rep., no 2, Electr. Lab. University of Innsbruck, Austria.

Gurin, G., Tarasov, A., Ilyin, Yu. & Titov, K., 2013. Time domain spectral induced polarization of disseminated electronic conductors: laboratory data analysis through the Debye decomposition approach, *J. appl. Geophys.,* **98,** 44–53.

Gurin, G., Tarasov, A., Ilyin, Y. & Titov, K., 2014. Application of the Debye decomposition approach to time domain induced polarization profiling data: an ore exploration example, in *Proceedings of the 3rd International Workshop on Induced Polarization,* pp. 104–105, Ile d'Oleron, France, 6–9 April 2014.

Hanai, T., 1968. Electrical properties of emulsions, in *Emulsion Science,* pp. 353–478, ed. Sherman, P.H., Academic Press.

Hofstra, A.H. & Cline, J.S., 2000. Characteristics and models for Carlin-type gold deposits, *Rev. Econ. Geol.,* **13,** 163–220.

Hubbard, C.G., West, L.J., Rodriguez-Blanco, J.D. & Shaw, S., 2014. Laboratory study of spectral induced polarization responses of magnetite—Fe^{2+} redox reactions in porous media, *Geophysics,* **79,** D21–D30.

Ilyin, Yu.T., 1968. Elektrokhimicheskie svoistva nekotorykh margantsevykh mineralov I rud (Electrochemical properties of some manganese minerals and ores) Vestnik LGU, Seria Geografia I Geologia, N 24, vypusk 4.

Ilyin, Yu.T., Sveshnikov, G.B. & Shtern, N.L., 1980. Elektrokhimicheskie svoistva prirodnykh elektronnykh provodnikov (Electrical properties of natural electronic conductors) Uchenye zapiski LGU, Seria Fisicheskikh I Geologicheskikh nauk, N 356, vypusk 20.

Kemna, A., 2000. *Tomographic Inversion of Complex Resistivity: Theory and Applications,* Der Andere Verl.

Kemna, A. *et al.*, 2012. An overview of the spectral induced polarization method for near-surface applications, *Near Surf. Geophys.,* **10,** 453–468.

Kormiltsev, V.V., 1980. *Perehonie processi pri vizvanoy polarizacii,* Nedra Press, 112 pp. (in Russian).

Leroy, P., Revil, A., Kemna, A., Cosenza, P. & Ghorbani, A., 2008. Complex conductivity of water-saturated packs of glass beads, *J. Coll. Interface Sci.,* **321,** 103–117.

Lesmes, D.P. & Frye, K.M., 2001. Influence of pore fluid chemistry on the complex conductivity and induced polarization responses of Barea sandstone, *J. geophys. Res.,* **106**(B3), 4079–4090.

Mahan, K.M., Redman, J.D. & Strangway, D.W., 1986. Complex resistivity of synthetic sulphide bearing rocks, *Geophys. Prospect.,* **34,** 743–768.

Mansoor, N. & Slater, L., 2007. On the relationship between iron concentration and induced polarization in marsh soils, *Geophysics,* **72,** A1–A5.

Marshall, D.J. & Madden, Th.R., 1959. Induced polarization, a study of its causes, *Geophysics,* **26,** 790–816.

Morgan, F.D. & Lesmes, D.P., 1994. Inversion for dielectric relaxation spectra, *J. Chem. Phys.,* **100**(1), 671–681.

Nelson, P.H. & Van Voorhis, G.D., 1983. Estimation of sulfide content from induced polarization data, *Geophysics,* **48,** 62–75.

Nordsiek, S. & Weller, A., 2008. A new approach to fitting induced-polarization spectra, *Geophysics,* **75**(6), F235–F245.

Ntarlagiannis, D., Doherty, R. & Williams, K.H., 2010. Spectral induced polarization signatures of abiotic FeS precipitation, *Geophysics,* **75,** F127–F133.

Pelton, W.H., Ward, S.H., Hallof, P.G., Sill, W.R. & Nelson, P.H., 1978. Mineral discrimination and removal of inductive coupling with multifrequency IP, *Geophysics,* **43,** 588–609.

Placencia-Gómez, E., Slater, L., Ntarlagiannis, D. & Binley, A., 2013. Laboratory SIP signatures associated with oxidation of disseminated metal sulffides, *J. Contam. Hydrol.,* **148,** 25–38.

Revil, A., Skold, M., Hubbard, S.S., Wu, Y., Watson, D.B. & Karaoulis, M., 2013. Petrophysical properties of saprolites from the Oak Ridge integrated field research challenge site, Tennessee, *Geophysics,* **78,** D21–D40.

Schlumberger, C., 1920. *Etude sur la prospection e´lectrique du sous-sol. Gauthier-Villar et Cie,* pp. 70–72, Chap. VIII, Gauthier-Villar et Cie.

Schwartz, G., 1962. A theory of the low frequency dielectric dispersion of colloidal particles in electrolyte solution, *J. Phys. Chem.,* **66,** 2636–2642.

Scott, W.J. & West, G.F., 1969. Induced polarization of synthetic, high-resistivity rocks containing disseminated sulfides, *Geophysics,* **34,** 87–100.

Sigel, H.O., Vanhalaz, H. & Sheard, N., 1997. Some case histories of source discrimination using time-domain spectral IP, *Geophysics,* **62,** 1394–1408.

Slater, L.D., Choi, J. & Wu, Y., 2005. Electrical properties of iron-sand columns: implications for induced polarization investigation and performance monitoring of iron-wall barriers, *Geophysics,* **70,** G87–G94.

Slater, L., Ntarlagiannis, D. & Wishart, D., 2006. On the relationship between induced polarization and surface area in metal-sand and clay-sand mixtures, *Geophysics,* **70,** A1–A5.

Suhotin, A.M., 1981. *Spravochnik po electrohimii,* Himiy Press, 488 pp. (in Russian).

Tarasov, A. & Titov, K., 2007. Relaxation time distribution from time domain induced polarization measurements, *Geophys. J. Int.,* **170**(1), 31–43.

Tarasov, A. & Titov, K., 2013. On the use of the Cole-Cole equations in spectral induced polarization, *Geophys. J. Int.,* **195,** 352–356.

Vanhala, H. & Peltoniemi, M., 1992. Spectral IP studies of Finnish ore prospects, *Geophysics,* **57,** 1545–1555.

Wait, J.R., 1958. A phenomenological theory of induced electrical polarization, *Can. J. Phys.,* **36,** 1634–1644.

Weller, A., Slater, L., Nordsiek, S. & Ntarlagiannis, D., 2010. On the estimation of specific surface per unit pore volume from induced polarization: a robust empirical relation fits multiple data sets, *Geophysics,* **750**(5), WA105–WA112.

Weller, A., Breede, K., Slater, L. & Nordsiek, S., 2011. Effect of changing water salinity on complex conductivity spectra of sandstones, *Geophysics,* **76,** F315–F327.

Wong, J., 1979. An electrochemical model of the induced-polarization phenomenon in disseminated sulfide ores, *Geophysics,* **44**(7), 1245–1265.

Wong, J. & Strangway, D.W., 1981. Induced polarization in disseminated sulfide ores containing elongated mineralization, *Geophysics,* **46,** 1258–1261.